ULUSLARARASI 3B YAZICI TEKNOLOJİLERİ
VE DİJİTAL ENDÜSTRİ DERGİSİ
INTERNATIONAL JOURNAL OF 3D PRINTING
TECHNOLOGIES AND DIGITAL INDUSTRY

ISSN:2602-3350 (Online)
URL: https://dergipark.org.tr/ij3dptdi

COMPARATIVE STUDY OF MATERIAL EXTRUSION AND VAT PHOTOPOLYMERIZATION ADDITIVE MANUFACTURING TECHNIQUE USING SQUARE BASE PYRAMID AS AN ARTIFACT AND APPLICATIONS

Yazarlar (Authors): Bhanu Prakash Bisht, Vijaykumar Toutam*, Sanjay R. Dhakate

Bu makaleye şu şekilde atıfta bulunabilirsiniz (To cite to this article): *Bisht B. P., Toutam V., Dhakate S. R., "Comparative Study of Material Extrusion and Vat Photopolymerization Additive Manufacturing Technique Using Square Base Pyramid as An Artifact and Applications" Int. J. of 3D Printing Tech. Dig. Ind., 8(3): 370-386, (2024).*

DOI: 10.46519/ij3dptdi.1540408

Araştırma Makale/ Research Article

Erişim Linki: (To link to this article): https://dergipark.org.tr/en/pub/ij3dptdi/archive

COMPARATIVE STUDY OF MATERIAL EXTRUSION AND VAT PHOTOPOLYMERIZATION ADDITIVE MANUFACTURING TECHNIQUE USING SQUARE BASE PYRAMID AS AN ARTIFACT AND APPLICATIONS

Bhanu Prakash Bisht [a, b], Vijaykumar Toutam [a, b *], Sanjay R. Dhakate [a, b]

[a]Academy of Scientific and Innovative Research (AcSIR), CSIR-National Physical Laboratory, Dr K. S. Krishnan Marg, New Delhi 110012, India.

[b]Advanced Materials and Device Metrology Division, CSIR-National Physical Laboratory, Dr. K. S. Krishnan Marg, New Delhi 110012, India.

[*] *Corresponding Author:* toutamvk@nplindia.org

(**Received:** 20.08.2024; **Revised:** 14.12.2024; **Accepted:** 16.12.2024)

ABSTRACT

A comparative analysis of Material Extrusion and VAT Photopolymerization 3D printing is done using various geometrical models, including square base pyramid, co-centric circular stamps, and lattice structures. The pyramid with Council of Scientific and Industrial Research (CSIR) and National Physical Laboratory (NPL) logos, texts printed by both techniques is studied for its dimensional accuracy as per the process parameters. The 3D printed specimen by Material Extrusion measured an average layer thickness of ~ 104 µm and VAT Photopolymerization measured a layer thickness of ~ 54 µm. The calculated void volume of the printed pyramid due to the staircase effect is ~ 2.9 % for the Material Extrusion and ~ 0.14 % for the VAT Photopolymerization. Mechanical properties of ASTM D638 tensile test samples based on build orientation showed anisotropy for Material Extrusion, whereas VAT Photopolymerization printed test samples are isotropic. The degree of anisotropy (DOA) of 0.35, modulus of elasticity (MOE) of 1.7 GPa and ultimate tensile strength (UTS) of 62 MPa are measured for the Material Extrusion printed test sample. The ZXY build-oriented test sample showed the lowest values compared to all the other build orientations. Comparatively, the MOE and UTS for the VAT Photopolymerization printed samples are equal for all build orientations and are ~ 950 MPa and ~ 39 MPa, respectively. The applicability of the present comparison of 3D printing techniques is demonstrated through functionality studies of printed stamps for ring electrodes and lattice structures as templates. The active area of the Fused deposition modeling (FDM) printed ring electrodes for maximum resolution is 17 times larger compared to that of Digital light processing (DLP) printed stamps. Additionally, the mean pore size for FDM-printed lattice structures was found to be ~ 650 µm, while the lattice structure printed by DLP using Polyurethan acrylate resin exhibited a pore size of ~ 220 µm. This analysis evaluates the dependence of stamp size due to print resolution specific to the technique. The importance of this research lies in addressing the growing demand for optimized 3D printing processes in manufacturing applications, such as sensors, electrodes, and structural components. By comparing dimensional accuracy, surface finish, print resolution, and mechanical properties, this study offers valuable insights into how the selection of printing techniques and process parameters can significantly influence the final product's performance.

Keywords: Additive Manufacturing, Staircase Effect, Build Orientation, Test Artifact, FDM Vs DLP, Printing Parameters, Ring Electrode.

1. INTRODUCTION

Additive Manufacturing (AM) is a freeform, direct digital, rapid, and additive fabrication of prototypes, tools, patterns, and concept parts as well as functional devices for direct application and service as per American Society for Testing and Materials (ASTM) F42 Technical Committee [1]. As per ASTM 52900:2021, additive manufacturing is categorized into seven distinct processes; binder jetting, directed

energy deposition, material extrusion, material jetting, powder bed fusion, sheet lamination, and vat photopolymerization [2]. For the application and functionality of the printed models and for industrial production, certain criteria should be met, like surface finish, dimensional tolerance, mechanical properties, density, physical, and chemical properties [3].
Fused deposition modeling (FDM), based on material extrusion, is the most widely practiced additive manufacturing (AM) technique, involving precisely controlled layer-by-layer deposition of thermoplastic polymer through a heated nozzle. This method produces objects with a dimensional accuracy of the order ~100 µm by extruding molten material onto a build stage, where it solidifies and forms layers that adhere together [4].

Despite its simple process and moderate accuracy, FDM competes with alternative polymer-based AM technologies such as Powder Bed Fusion (PBF) and VAT photopolymerization (VPP). Due to its ease of deposition and accessibility, a variety of feedstock materials have been developed and are still emerging. Starting from basic thermoplastics like Polylactic acid (PLA) and Acrylonitrile butadiene styrene (ABS) and engineered plastics like Polyether ether ketone (PEEK) and Polyetherimide (PEI) to biopolymers, the library of materials is huge [5]. It caters needs of several industries like prosthetics, implants, and surgical tools in the medical industry [6], functional and carbon composites for energy storage [7], sensors [8], biopolymers for tissue engineering, and prototype designing of several components in the aeronautical and automobile industries [9].

Despite several advantages associated with the FDM technique and its application for several fields, the technique suffers from poor surface finish, weak mechanical strength of build parts, and build orientation-dependent anisotropy in physical and mechanical properties. These drawbacks are mostly related to the method of deposition [10]. The layer-by-layer deposition makes volumetric gaps on the surface and internal filling. The build orientation brings structure instability along one axis, and the viscoelastic nature of the polymer during extrusion brings interfacial bond instability based on the temperature of extrusion and speed. Also, the dimensional accuracy is influenced by print speed, nozzle, and bed temperature [11].

VAT Photopolymerization (VPP) based AM technique creates 3D models by selectively curing a resin, layer by layer in a VAT using a light source forming complex geometries with very high resolution [12]. Digital light processing (DLP) is a preferred choice for creating 3D models with applications requiring complex geometries and intricate features with high resolution, speed, and smooth surface finish [13]. Unlike FDM, DLP prints 3D models by curing each layer through flash projection rather than mechanical movement. This effectively reduces the complexity of printing. Also, resolution of less than 50 µm can be achieved with great and intricate details [14]. The curvature effects and voids seen in FDM printing are eliminated largely by this mode of printing. Different resins starting from standard, structural to elastomeric resins are available as per application [15]. Resins being in liquid form can be easily mixed with several additives like nano-powders, carbon, and ceramic materials making composites for 3D printing [16]. Despite these advantages, resin printing is limited only to prototyping in fields like dentistry, jewelry, and medical implants and applications in antenna designing and fabrication, low to high dielectric materials for the electronic industry [17-18]. The feasibility of printing multi-materials using VAT photopolymerization has also hindered the advancement of this technique. The resin material used for printing is thermosetting which is brittle in nature and has mechanical properties not suitable for fatigue, wear, and tear [19]. It offers fewer material options than other 3D printing technologies. Post-processing requirements can be complex and time-consuming. The disposal of unused resin, and handling chemicals and photopolymer components raises environmental problems [20].

To print a quality product in terms of dimensional accuracy and mechanical stability by additive manufacturing, 3D printer, and process parameters must be optimized. For 3D printing, hardware conditions like tolerances of stepper motors, load bearing of the gears and railing, and thermal expansion of material used for building printers play major roles in the reproducibility of printed parts [21]. This is

generally optimized by the manufacturer of the machine. At the user end, process parameters play a crucial role in the dimensional tolerance and surface finish of the printed models. There are several process parameters that can be optimized when it comes to FDM like layer thickness, layer/raster width, raster angle, printing speed, nozzle and bed temperature, build orientation, infill pattern, infill percentage, and outer layers [22].

Ferretti P et al. established a relation between optimization for fabrication of lower defect-free 3D models [23]. Gao X et al. highlight the mechanical anisotropy of FDM-printed parts by changing the raster angle and build direction [22]. Bakhtiari H et al. study the influence of FDM printing parameters on the compressive properties and surface roughness of PLA specimens [24]. Bouzaglou O et al. studied the effect of material selection, printing factors such as path (layer thickness and raster angle), build (infill and building orientation), and temperature parameters (nozzle or bed temperature) on mechanical properties [25]. Many of the researchers worked on the Design of experiment (DoE) such as the Taguchi method, full factorial, and response surface methodology (RSM) for optimizing the process parameters and minimizing the number of experiments [26].

Factors affecting DLP printing are divided into two categories: one is related to the machine, and the other is related to the photocurable resin. Machine-related parameters are layer thickness, light emitting diode power, flux uniformity, etc. Resin-related parameters are penetration depth, critical energy, viscosity, etc. Brighenti R et al. showed the printing process parameters of DLP on mechanical characteristics and concluded that the built specimen strength is dependent on the post-printing curing process [27]. Zhang Z et al. investigated the effect of printing layer thickness on model accuracy and found that decreasing the layer thickness from 0.10 mm to 0.05 mm increases the accuracy of the DLP 3D printing model [28]. Jiang T et al. studied the forming performance and characteristics and found that as the layer thickness increases from 0.02 to 0.22 mm, the dimensional accuracy first increases and then decreases for the DLP printed specimen [29]. Sector wise strength and weakness of FDM and DLP printing have been shown in Table 1.

Table 1: Sector wise strength and weakness of FDM and DLP printing.

Sector	FDM	DLP
Automotive & Aerospace	Cost-effective for large prototypes and functional parts. Suitable for jigs, fixtures, and custom tools.	Limited in large-scale parts. Ideal for precision components like small gears, valves, and aesthetic parts.
Medical Devices	Used for creating medical models and prosthetics.	Superior for micro-scale medical devices like dental molds, surgical guides, and hearing aids.
Consumer Goods & Electronics	Useful for rapid prototyping of large consumer products.	Ideal for small, high-detail items like phone cases, wearables, and electronic housings. High precision enables creation of detailed product designs for miniaturized electronics.
Jewelry & Fashion	Limited use due to lack of fine detail. More useful for accessory molds or larger costume designs.	Preferred for small, intricate designs like rings, necklaces, and detailed accessories.
Architecture & Construction	Useful for printing large architectural models and prototypes. Suitable for scaled-down models of buildings and construction elements.	Best suited for fine-scale models that require accurate texture and finish (e.g., window grills, facades).
Education & Research	Accessible, low-cost solution for teaching, student projects, and early-stage R&D. Suitable for rapid prototyping and model validation.	Excellent for research requiring micro-precision components. Suitable for academic research focusing on photopolymers and high-detail components.

As 3D printing is accomplished through layer-by-layer deposition and needs a file understandable by the printer, the CAD model must be tessellated. For this, the 3D model is converted to an STL file so that the printer can slice and convert it to the G-code file, the machine language that the printer can understand. Inherently the process induces several defects like chordal effect during tessellation and staircase formation for oblique and curved surfaces due to layer-by-layer deposition along with air gaps and many other voids due to raster angle and infill pattern [30]. Both the FDM and DLP techniques show the staircase effect, and it can be minimized by decreasing layer height. As the typical feature resolution of FDM is 100-150 µm and for DLP it is 50-100 µm, the staircase effect is more prominent in FDM printed models as compared to DLP printed models [31].

From molecular structures in chemistry, architectural marvels like Egyptian pyramids, and the construction of other polyhedral, square pyramids form the basic building block [32]. It is also used to represent the hierarchy in ecology [33]. When it comes to standards in physical measurements, it represents measurement traceability for an unbroken chain of measurement for quality. The traceability pyramid creates an efficient and economical way for each lab or individual to access calibration standards.

A square pyramid has five vertices, eight edges, and five faces with four isosceles triangles making dihedral angles with the center line passing through the base [34]. These slant triangular faces are good for studying layer-by-layer deposition in terms of understanding the effect of these process parameters on surface roughness, dimensional accuracy, volumetric voids, and staircase effects. Even though there are in-depth studies and detailed reviews on FDM process parameters optimizing the dimensional accuracy and physical properties and very few studies on DLP process parameters for optimization of conditions for accurate 3D printed models. Except for the NIST test artifact which studied the dependence of process parameters for both the techniques independently, there are not many studies comparing both the techniques and the dependence on process parameters for dimensional tolerances, surface roughness, print resolution, and mechanical anisotropy of the 3D printed models (Table 2).

Table 2: The different artifacts used in literature for optimization of printing parameters.

Tech.	Parm.	Artifact	Output	Ref
FDM	Layer thickness	Pyramid, cube, and hemisphere over a platform	Surface quality, shear, and tensile strength, build time, accuracy, and precision	[35]
FDM	Printing speed, Layer height	ISO ASTM 52902-2021 specimen feature with coarse resolution holes	Geometrical Accuracy	[36]
FDM and DLP	-	NIST standard test artifact	Dimensional Uncertainty quantification	[37]
DLP	Exposure time	Orthogonal test samples, flowers with cylindrical small features	Resolution	[38]
DLP	Separation force	Cylindrical geometry, Lattice structure	Cross-section geometry and separation speed	[39]
FDM and DLP	-	Dental model	Trueness and precision	[40]
FDM and DLP	Printing speed, Exposure time	Square base pyramid artifact	Roughness, dimensional accuracy, surface finish, print resolution	In this work

In the present study, we investigated the 3D-printed square base pyramid with Council of Scientific and Industrial Research (CSIR) and National Physical Laboratory (NPL) logos and texts on triangular facets for comparative analysis and standardization of Material Extrusion and VAT photopolymerization AM techniques. We compared both techniques with respect to the layer thickness, edge sharpness, text resolution, and staircase effect. We also

studied interlayer bonding and mechanical strength based on build orientation through stress-strain analysis using standard tensile test samples and analyzed the uniqueness and versatility of both the techniques. To compare and study the dependence of print resolution, tolerances, and uniformity on the functionality of 3D printed models by both the techniques, two case studies, one using ring electrode stamps and the other using lattice structure have been demonstrated and analyzed.

2. MATERIAL AND METHODS

3D printing of square base pyramids with CSIR, NPL logos, and text is done by adopting FDM and DLP printing techniques. A 3D printer having a Hamera-based all-metal dual extruder is used for FDM-based printing of pyramids. The printer has a large build volume of 300 × 300 × 500 mm^3 and the capability of high-temperature extrusion up to 400 °C. For DLP printing, an LD-002R resin printer by Creality containing a VAT of build volume of 120 × 65 × 165 mm^3 and a UV LED of 405 nm wavelength and 30 W power is used. For post-processing of printed resin models, a UW-01 washing and curing is used.

Polylactic acid (PLA) spool from Sigma-Aldrich is used for FDM printing and Polyurethane acrylate (PUAR) resin bought from Anycubic is used for DLP 3D printing. For slicing and setting process parameters during 3D printing, Simplify3D slicer software for FDM and Chitubox for the DLP technique is used.

STL files of text and logos of both CSIR and NPL and a square-base pyramid are used for 3D printing. The size of the square-based pyramid is 5 cm^3. Arrangement and orientation of STL files of individual logos and text onto the triangular faces of the square base pyramid are done using the gizmos option available in Simplify 3D. A layer thickness of 100 µm is chosen as it offers a balance between print quality and speed [31]. A rectilinear infill pattern with 100% density is chosen to improve the strength of printed parts. A speed of 60 mm/sec to improve the dimensional accuracy and print resolution. Extrusion multiplier is adjusted to 0.9 to avoid over deposition and match with the speed of printing [41]. As PLA is used for FDM printing, an extruder temperature of 200 °C and bed temperature of 50 °C are used as printer parameter settings during slicing. Similarly, for DLP resin printing, the optimized process parameters are 50 µm layer height as it is minimum lift possible with stepper angle of the stepper motor, being a flash printing technique, the infill density is 100 % by default. For proper adhesion to the build plate an initial layer exposure time of 50 sec first 8 layers followed by 6 sec for rest of the layers is chosen [42]. Table 3 below summarizes all the process parameters used for 3D printing of the CSIR-NPL pyramid and their comparison for both the FDM and DLP printing techniques.

Standard tensile test samples are fabricated by both the FDM and DLP techniques for studying mechanical properties. Tensile specimens were made in accordance with the ASTM D638 (Type IV) standard, with dimensions of length 115 mm, width 19 mm, thickness 4 mm, and waist length 32 mm. The samples were tested till failure to investigate their mechanical properties.

Concentric ring electrode stamps were modeled using Blender. Three different sizes, small (S), medium (M), and large (L) are made to ensure optimal resolution for both FDM and DLP 3D printing techniques. Lattice structrue of 1 × 1 cm^2 are printed by both FDM and DLP technique. Similar process parameters optimzed for printing square base pyrmaid are used for printing ring electrode stamps and lattice structures.

Microscopic analysis of printed models is done using an MX6R optical microscope by AmScope Ltd. The layer height distribution is done using the stylus profilometer, Ambios, model XP-200 with a tip diameter of 2.5 µm and tip force of 1.9 mN. La Jarden clay is used for taking imprints of the triangular face edges for their sharpness study. Image J software is used for the edge sharpness and layer thickness. The mechanical testing of FDM and DLP printed test samples is done using universal testing machine, Instron 5967 with a load measurement accuracy of ± 0.5% having a capacity of 5 kN.

3. RESULT AND DISCUSSION

3.1. Slicing and Process Parameters

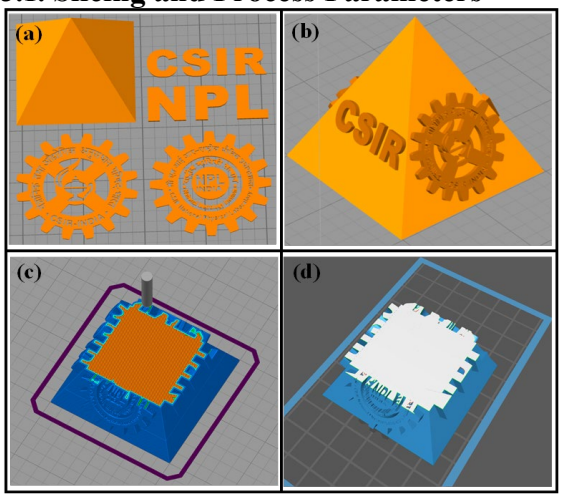

Figure 1: STL files of CSIR, NPL logos, text, and the CSIR-NPL pyramid, and the sliced images of the pyramids for FDM and DLP printing. (a) STL files of the square base pyramid and individual STL files of logos and text files, (b) STL file of merged CSIR-NPL pyramid. Image of pyramid sliced in slicer software (c) Simplify 3D (d) Chitubox.

Figure 1 shows the STL files of the CSIR-NPL pyramid with individual files consisting of CSIR, NPL logos, their text files, and the square pyramid along with the slicing of the combined STL files required for both the FDM and DLP techniques.

Figure 1a shows the individual STL files of the CSIR-NPL pyramid. Logos required for the creation of the STL file are taken from the following web links [43-44]. These image files are saved as JPG files and are converted to scalar vector graphic (SVG) files using the image online converter. The text files are created using PowerPoint and are converted to JPG and further into SVG files [45]. The square pyramid used for this study is taken from Thingiverse [46]. All these SVG files are converted into STL files using the svg2stl converter [47].

Figure 1b shows the unified STL file of the CSIR-NPL pyramid with logos and text files aligned onto the triangular faces of the square pyramid. These individual files are partially embedded into the square pyramid to avoid the separation of these from the pyramid during slicing, and to optimize the printing parameters. The 3D printed pyramid used for the current study is of dimensions with a square base of 5 cm and a vertical height of 5 cm.

The orientation of all logos and text files with the face of the pyramid is done in the slicer software. In the present case, all the logos and text STL files are aligned onto the faces of the pyramid and are exported into a single STL file, ready for slicing. 'Allow single extrusion' of the thin wall behavior option available in slicer software is used such that the gap in the narrow regions is filled with a single extrusion layer rather than raster infill where regular infill is not possible. This allows improvement in the resolution of printing, and smoothness. The small text found in logos can also be printed using this option.

Figures 1c and 1d show the slicing of the CSIR-NPL pyramid STL file generating G code files required for both the FDM and DLP printing. Table 3 summarizes all the process parameters used for 3D printing of the CSIR-NPL pyramid and their comparison for both the FDM and DLP printing techniques.

Table 3: Comparison of printing parameters of FDM and DLP printed 3D pyramid.

Parameters	FDM	DLP
Machine	Hamera all metal extruder printer	Creality LD-002R
Material	PLA	PUAR Resin
Slicer	Simplify 3D	Chitubox
Layer height	100 µm	50 µm
Infill pattern	Rectilinear	Complete fill
Infill percentage	100 %	100 %
Speed	60 mm/s	6 sec/layer
Time	6 h 50 min	3 h 30 min
No. of outer walls	3	-
Top/bottom layer	5	-
Extrusion multiplier	0.90	-
Nozzle travel speed (XY)	120 mm/s	
Bottom layer count	-	10
Bottom layer exposure time	-	60 s
Other layer exposure time	-	6 s
Lift up speed	-	65 mm/min
Lift up distance	-	5 mm

3.2. Layer Thickness

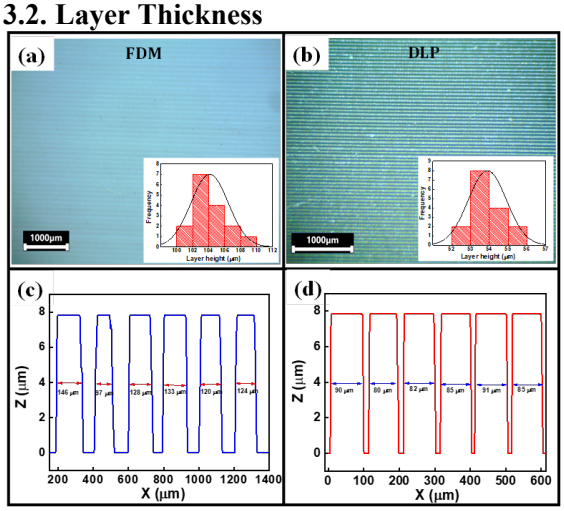

Figure 2: Optical image and statistical distribution of layer height, stylus profilometry measurement of FDM and DLP printed pyramid. Optical image of layer profile of (a) FDM, (b) DLP printed samples, and inset showing their thickness distribution respectively; Stylus profilometry analysis of (c) FDM and (d) DLP printed samples.

For a detailed analysis of the layer thickness of the FDM and DLP printed models, the surface of the 3D-printed pyramid is analyzed for their layer width and uniformity. Figure 2 shows the optical images of the face of the pyramid showing layers, along with profile analysis. Figure 2a shows the optical image of the printed layers by FDM along with the distribution analysis as shown by the histogram in the inset. From the histogram analysis, the layer width is estimated to be ~ 104 µm with a standard deviation of 5 %. Similarly, Figure 2b shows the optical image of the printed layers on the face of the pyramid printed by the DLP technique and the histogram analysis. From the above analysis, the layer width is found to be ~ 54 µm with a standard deviation of 4 %.

Figure 2c and 2d shows the stylus profiling of the surface shown in Figures 2a and 2b. The average width of the layers of the FDM printed pyramid measured is ~ 130 µm and that of the resin printed pyramid is ~ 85 µm. From the above profiles, the layer width and distribution are more compared to that of optical image and histogram analysis. This increase in width is attributed to the tip convolution effect of the stylus profiler. Also, the layer height from the stylus profiler, which corresponds to roughness is the same for both the FDM and DLP printed models. Even though the DLP printed models have lower layer thickness and less distribution, due to the tip with a large area of cross-section, the tip convolution during stylus profilometry won't be able to resolve the roughness variations. Also, it can be observed that the layer width is uniform, and the resolution is better for DLP printing by 50%. This establishes the superiority of the DLP technique over the FDM technique for smoothness, resolution, and surface finish [48]. The finer layer width and high resolution achieved with DLP printing make it ideal for industries requiring detailed and precise surface finishes, such as medical devices, and jewelry where intricate and uniform designs are essential. In contrast, FDM technique, despite its larger layer width, makes it suitable for applications in architecture, construction, automotive, and aerospace sectors [7-9].

3.3. Edge Sharpness And Print Resolution

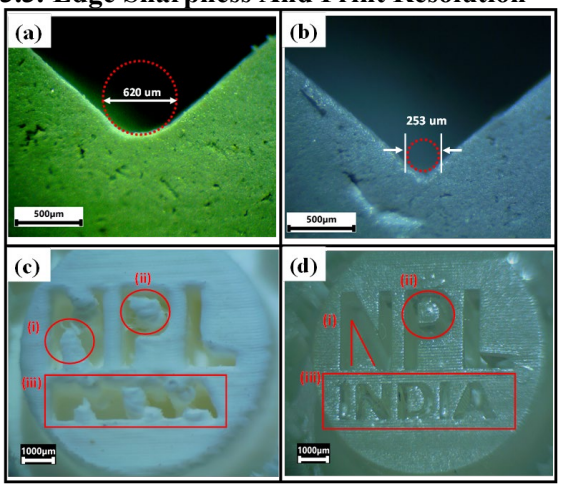

Figure 3: Edge sharpness measurement and print resolution of FDM and DLP printed pyramids: Optical image of imprint of the edges of the pyramid taken using molding clay (a) for FDM printing, (b) for DLP printing. Text resolution of the NPL logo (c) by FDM, and (d) by DLP.

Figures 3a and 3b show the sharpness of the edges of the pyramid. As FDM is a mechanical movement-based extrusion printing, during slicing, the tessellation is done such that there is a coordination between extrusion speed and the movement of the nozzle. This coordination makes the tip move slowly at the edges and the contours have a more circular finish/edges [11]. Figure 3a shows the optical image of the edge imprint taken using the clay molding technique. From the optical image, the convergence of two faces has a wide rounding with a diameter of 620 µm.

Figure 3b shows the optical image of the face edge imprint taken for the DLP-printed pyramid. In comparison to edge sharpness for FDM, the convergence of two faces of the DLP printed pyramid has a sharp edge with a sharpness cross-section of 253 µm as shown in Figure 3b. As DLP printing is a flash printing technique where the whole layer of the model is printed in a flash by curing the resin using UV light, the edges are defined thoroughly, and the resolution and the sharpness of the edges are high. From the above comparison, it is observed that the FDM-printed pyramid is more rounded at the edges of the faces compared to the DLP-printed pyramid and is 150% more rounded at the edges.

Figures 3c and 3d show the resolution of the small text achieved under FDM and DLP printing. In similar lines about the behavior of the nozzle movement compared to flash printing of the DLP technique, the text is well defined in DLP printing compared to FDM printing [49], [50]. Allow single wall extrusion to a certain extent improves the resolution of the text printed by FDM. Also, the resolution in LCD-based DLP printing, decided by the pixel density, is proven to be better compared to the extrusion-based FDM printing. From Figure 3d (iii) compared to 3c (iii), the text with a smaller font 'INDIA" is better resolved in the DLP model. Also, the edge sharpness of the letter 'N" can also be distinguished clearly in DLP printing compared to FDM as observed in Figure 3c (i) and 3d (i). The superior sharpness possible with DLP finds applications in designing fine features in biomedical fields like microfluidic channels, and artificial organs. Whereas FDM is useful for rapid prototyping of large consumer products [6, 49, 51].

3.4. Build Orientation and Its Effect On Mechanical Properties

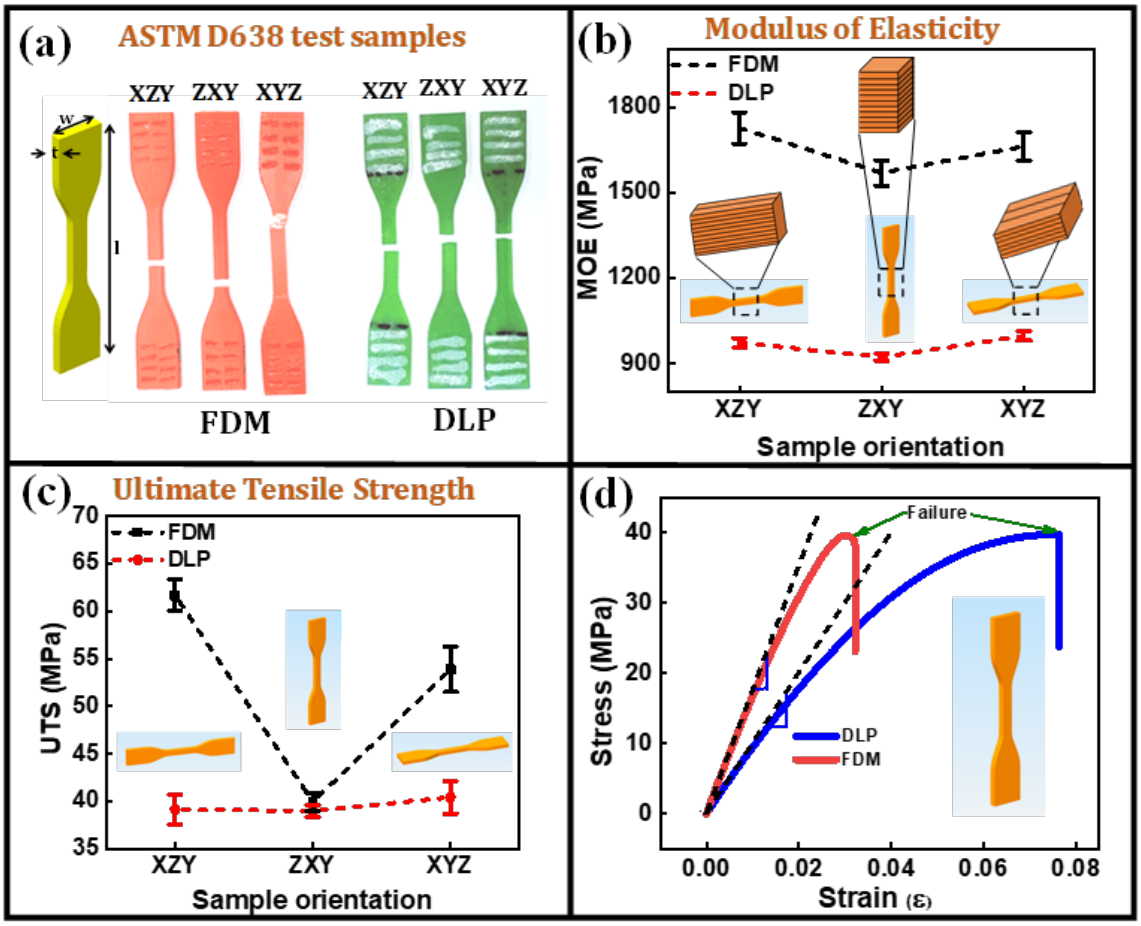

Figure 4: The image of ASTM D638 tensile test samples, Modulus of elasticity (MOE), Ultimate tensile strength (UTS), and stress-strain analysis of the FDM and DLP printed specimens. (a) Image of ASTM D638 sample after testing, (b) MOE, (c) UTS of samples printed in different orientations on the build plate, and (d) The stress vs strain analysis of vertically printed FDM and DLP test sample.

Figure 4 shows the comparison of the mechanical properties of both the FDM and DLP printed tensile test samples and the effect of build orientation on these properties. Figure 4a shows the optical image of tensile test samples printed by both the FDM and DLP techniques with three axes of build orientation namely XZY, ZXY, and XYZ respectively where the long axis is represented by the first letter of the notation followed by preceding long axes as per the nomenclature followed by ASTM 52921:2021 standard [52]. From the image, it can be observed that all the samples are tested for their tensile strength and are subjected to breaking and the breaking of all the samples has happened across the waist. Figures 4b and 4c show the modulus of elasticity (MOE) and ultimate tensile strength (UTS) of FDM and DLP printed test samples. Figure 4b shows the plot of MOE with respect to build orientation for both FDM and DLP test samples. The schematic of the test samples represents their build orientation during printing. The zoomed inset from the waist of the schematic depicts the orientation of printed layers with respect to the build platform. From the inset, it can be observed that for FDM, the XZY sample has layer-by-layer deposition in the ZY plane along the width (w) with the infill along the length. For the XYZ test sample, the layer-by-layer deposition is along the thickness (t) of the sample with infill along the length. Equivalently, the XZY sample has more filaments stranded and aligned along the length compared to that of XYZ. This makes the test sample with XZY orientation having MOE and UTS large compared to the XYZ FDM test sample. Whereas the ZXY test sample of FDM has low MOE and UTS compared to the other two orientations due to layer-by-layer deposition along the length in the z-direction having low interlayer bond strength compared to XZY and XYZ-oriented test samples. For DLP printed test samples, the MOE is low compared to FDM test samples and is equal for all build orientations. Figure 4c shows the UTS plot with respect to the build orientation for both FDM and DLP test samples. In summary, it can be observed that MOE and UTS for the FDM test samples are maximum for XZY orientation, followed by XYZ orientation, and least for ZXY orientation [53]. Whereas the MOE and UTS for the DLP printed samples are almost equal for all build orientations [54]. The MOE and UTS of XZY and XYZ FDM test samples are ~ 1.7 GPa, 62 MPa respectively, whereas the ZXY test sample has MOE and UTS ~ 1.5 GPa, 40 MPa respectively [55]. The UTS of the ZXY FDM test sample is similar compared to that of the UTS of DLP test samples ~ 40 MPa. Also, the MOE and UTS of DLP test samples are similar irrespective of build orientation, hence the tensile properties are isotropic for DLP test samples. The anisotropy in tensile properties for FDM printing is attributed to the dependence on build orientation and can be measured quantitatively by the degree of anisotropy (DOA) represented by D_a. DOA is given by the percentage of the difference between the maximum and minimum UTS and, is calculated following the equation: $D_a = [(UTS_{XZY} - UTS_{ZXY}) / UTS_{XZY}] \times 100\%$ [22]. The DOA for the FDM printed model is calculated to be 0.35 and for the DLP printed model is 0.0035. The near-zero value for DOA of DLP test samples establishes that DLP-printed 3D models have low MOE and UTS with isotropic behavior irrespective of build orientation as compared to FDM-printed models. As layer-by-layer deposition is normal to the print direction for ZXY samples of both the FDM and DLP test samples, this build orientation is suitable for comparison of interlayer bonding by both techniques. Figure 4d shows the stress-strain curves of tensile test samples printed with ZXY orientation. From Figure 4d, both the samples show equal tensile strength at the maximum load which suggests that the interlayer bonding is equal for both the FDM and DLP printed test samples. It can also be observed from the stress-strain curves that DLP printed test samples have a breaking point without any yield whereas FDM printed test samples undergo yielding beyond the strain of 0.02 and have yield over an elongation of 4 % before breaking. In the case of the FDM printed sample, for the layer-by-layer deposition of fused thermoplastic, the interface between the layers is decided by both the layer thickness and raster width. Whereas for DLP printing, the curing of photopolymer takes place both in-plane and along normal. As the polymer entanglement is more in the DLP sample and isotropic [56], [57], it shows plastic behavior from the beginning with more strain and undergoes failure abruptly at maximum tensile stress. Hence the DLP printed test sample is more brittle than the FDM sample. The ultimate tensile strength calculated from the stress-strain curves for both the FDM and DLP test samples is ~ 40 MPa. The high anisotropy of FDM-

printed parts, along with a higher modulus of elasticity, makes FDM suitable for applications that require strength along specific orientations, such as load-bearing parts, test jig in automobile, and aerospace industry. Whereas DLP-printed parts, being isotropic, offer uniform mechanical properties in all directions, making them ideal for applications requiring consistent strength and flexibility across different orientations, such spare parts for automobile industry, and consumer electronics [8, 58-59].

3.5. Staircase Effect and Surface Finish

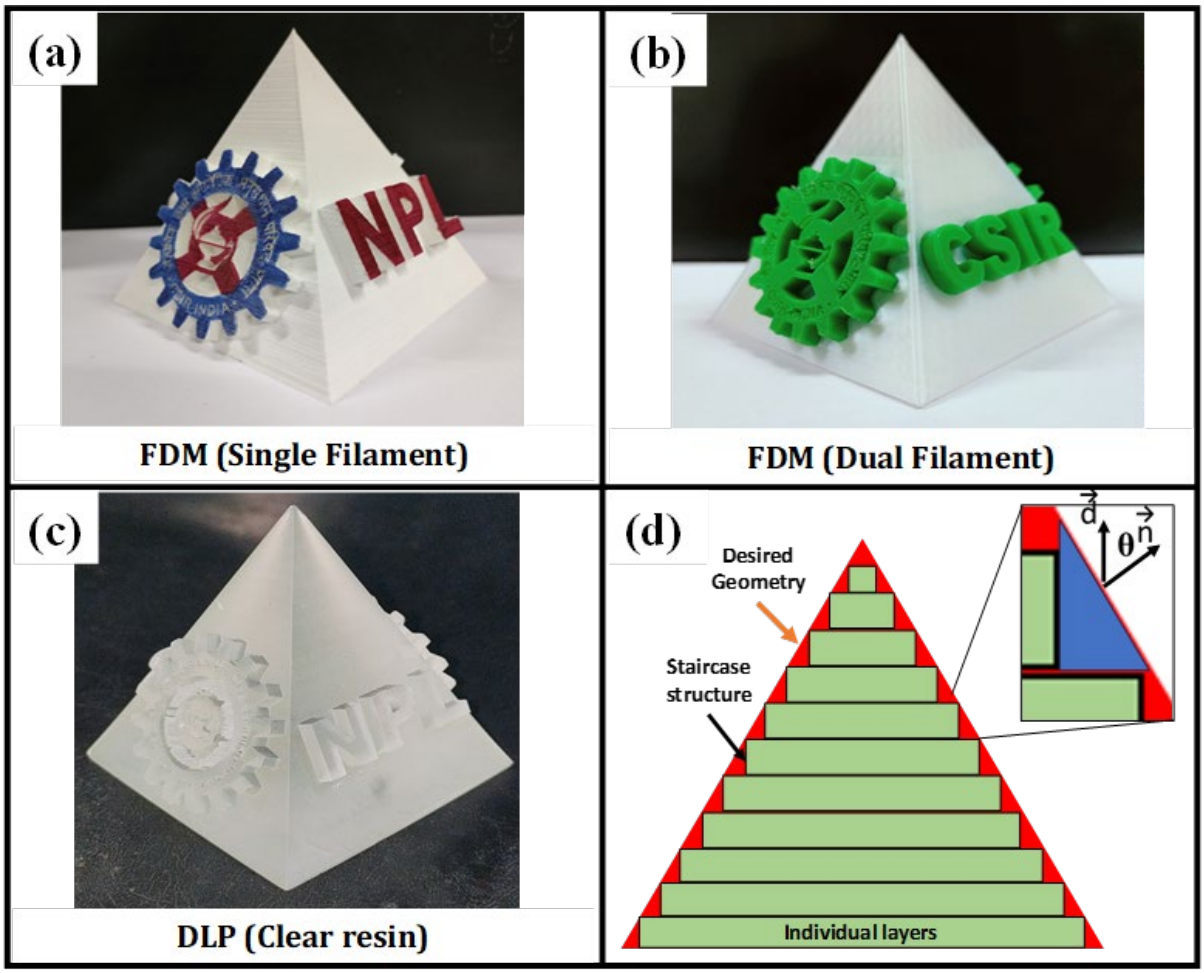

Figure 5: Image of 3D printed CSIR-NPL Pyramid printed using single filament, dual filament FDM, and DLP 3D printer and the staircase effect analysis. Pyramid printed via (a) single filament FDM, (b) dual filament FDM printing, (c) DLP printing technique, and (d) schematic of staircase effect present in 3D printed models with inset showing one such staircase.

Figure 5 shows the image of 3D-printed pyramids with FDM and DLP techniques and the staircase effect. Figures 5a and 5b show the 3D printed pyramid by single filament and dual filament extrusion FDM respectively. Figure 5a shows the pyramid printed with PLA filament (white) and the logos colored with different colors. In single filament printing the printing process is simplified with a single STL file and the distinction between individual STL files will not be there. Figure 5b shows the pyramid printed with dual filaments of PLA (white and green). It shows the capability of multi-material printing with FDM, which is not possible with DLP resin printing. Also, the complexity of process parameters during slicing increases as the G-code is modified to control the movement of the dual head during printing. Figure 5c shows the pyramid printed by the DLP 3D printing technique using PUAR clear resin. Figure 5d shows the schematic of the staircase effect present in a 3D-printed pyramid along with the inset showing one such staircase. The actual pyramid from the STL file to be printed

is shown in the background with red color and the stacked layered pyramid shows the achievable model by 3D printing technique. The staircase effect comes into account when the surface of the build model is either oblique or circular with an angle, $0 < \theta < 90$ where θ is the angle between $\vec{n}$ and $\vec{d}$. $\vec{n}$ is normal to oblique/curved surface and $\vec{d}$ is the vector normal to the build plate.

Based on layer thickness and tessellation density, the volume error can be calculated. For the present 3D pyramid, the triangular surface has no curvature, and the tessellation is done such that the volume error is simply dependent on layer thickness. From the dimensions of the pyramid and layer thickness used for both FDM and DLP techniques, the offset of the layer for each step resulting in the staircase effect is calculated to be 50 µm and 25 µm respectively. Based on this, the volume error between two layers is calculated. The estimated volume error following the process parameters for both FDM and DLP printed pyramids are 2.9 and 0.14 % respectively. Comparatively, the volume error for the DLP printed pyramid is low by 40 % of that of the FDM printed pyramid. This shows the higher surface finish and better print quality of the DLP-printed pyramid. DLP's low void volume and superior surface finish make it particularly suitable for applications in dental models, intricate jewelry, and biomedical application. Whereas, FDM having a higher void volume and visible staircase effect, is more appropriate for applications in architectural models, and industrial tools where the focus is on functionality and strength over aesthetic precision [54, 60].

3.6. Functionality Of Models Printed by FDM And DLP Technique

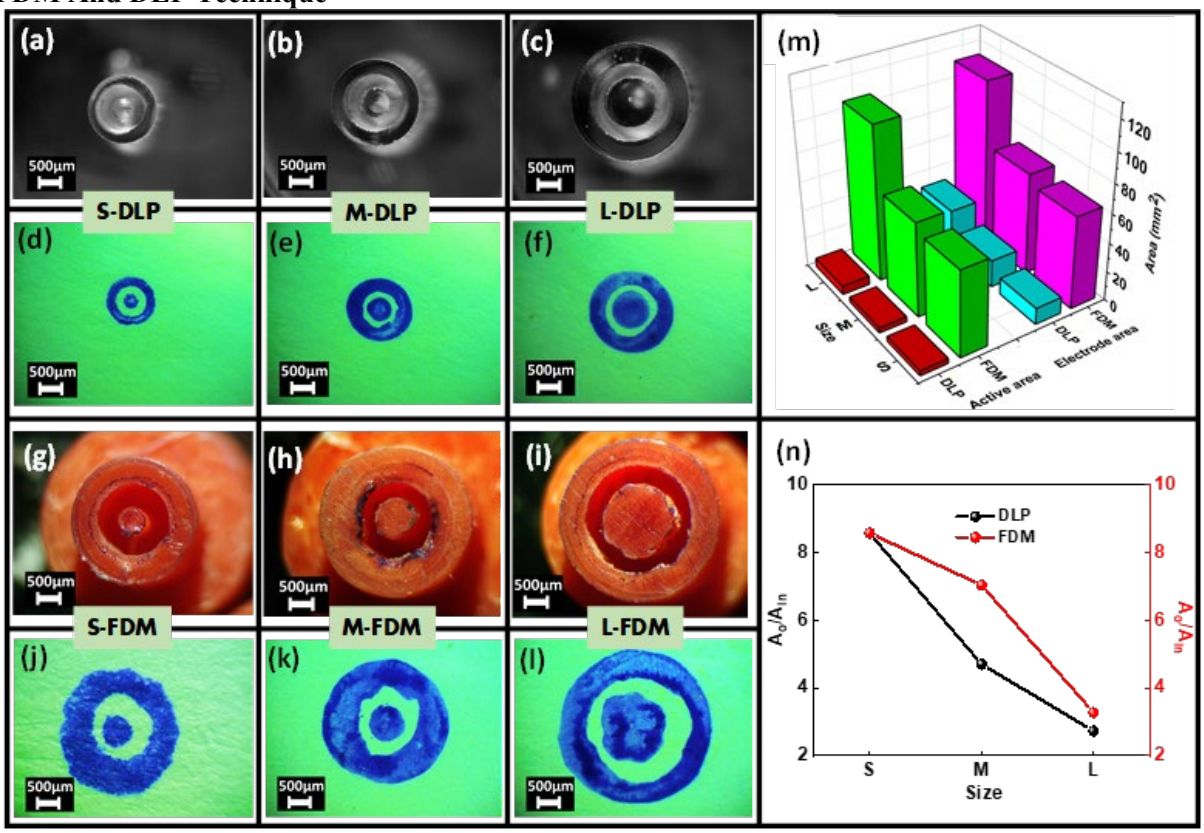

Figure 6: Stamps printed by DLP and FDM techniques along with co-axial ring electrode and their analysis. Stamps of different sizes (S, M, L) printed by DLP, Figures 6(a) – 6(c) and Figures 6(g) – 6(i) by FDM technique. Ring electrode imprints of DLP stamps, Figure 6(d) - 6(f) and FDM stamps, Figures 6(j) – 6(l). Figures 6(m), and 6(n) show the comparison of the active area, electrode area, and outer-to-inner electrode ratio of FDM and DLP printed stamps.

To understand the effectiveness of the present study, co-centric circular stamps of different sizes are printed using both techniques for the deposition of ring electrodes [61-62]. These ring electrodes find applications in sensors, LEDs, and memory devices [63-64]. Such co-

centric circular patterns can also be used in printing Fresnel lenses for optical devices and metamaterial applications [65]. Particularly for optical sensors, the behavior of the device is determined by the active area available for exposure to the incident light. The active area for ring electrodes is defined as the area available between two co-centric electrodes for external stimulation. Minimum, the active area, lesser the noise, higher the charge collection efficiency, and greater the responsivity. The size of the ring electrode decides the compactness and device density.

Figure 6 shows the co-centric circular stamp models printed using both FDM and DLP techniques and their imprint for ring electrodes. Figures 6a to 6c show stamps with three different sizes printed using the DLP technique denoted by S-DLP, M-DLP, and L-DLP, respectively. Similarly, Figures 6g to 6i show different-sized stamps denoted by S-FDM, M-FDM, and L-FDM, respectively, printed using the FDM technique. Both the S-DLP and S-FDM stamps are printed such that the printing conditions are optimized for the highest resolution possible with these printers. For DLP printed stamp, the highest resolution is achieved by optimizing the diameter of the inner circle through exposure time and lateral width determined by no: of excited pixels. Similarly, for FDM the highest resolution for the inner electrode is achieved by optimizing the minimum no: of strands required for printing. In the case of S-DLP and S-FDM, the optimized diameters achieved are 0.3 and 0.8 mm respectively. For determining the electrode size, the outer electrode diameter is considered, and the diameter of 1 and 3 mm is observed for S-DLP and S-FDM stamps respectively.

Figures 6d to 6f represent the ring electrode imprints produced by stamping all three DLP printed models from small to large, respectively using a blue dye. Similarly, figures 6j to 6l represent the ring electrode imprints produced by stamping FDM printed models. Active area, the size of the electrodes, and the ratio of the outer to inner electrode area are compared for both techniques to understand the functionality of the printed electrodes in terms of print resolution, uniformity, and roundness.

Figure 6m, shows the bar diagram analysis of both the active area and the outer electrode area of the imprints produced by stamps using both techniques. In the bar diagram, the grouping of both FDM and DLP for the active area and electrode size is shown along the x-axis. The y-axis represents three different-sized stamps for imprints and the z-axis represents the values of these parameters. From the analysis, it is found that the active area of the FDM imprints is 17 times larger compared to DLP-printed electrodes for all stamp sizes. Similarly, the size of the FDM-printed ring electrode is ~ 6 times that of the small stamp and 3.5 times that of the medium and large stamps printed by the DLP technique. Hence the device density of the DLP-printed ring electrodes can be 3 to 6 times larger compared to FDM-printed ring electrodes. This study emphasizes the importance of comparing both techniques to understand the functionality of printed models. Figure 6n compares the ratio of outer to inner electrodes of different stamps for both DLP and FDM techniques. From the analysis, it can be observed that the ratio for all the stamps for both techniques is the same, except for M-DLP and M-FDM where M-FDM is greater by 1.5 times. As the active area is proportional to stamp size, suggests that the outer electrode area is larger compared to other stamps.

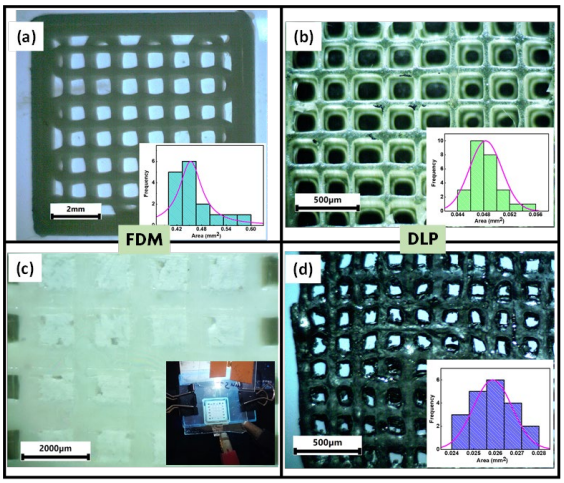

Figure 7: Functionality study of Lattice structure printed by FDM and DLP techniques. Lattice structure printed by (a) FDM and (b) DLP technique with inset showing the pore size distribution, (c) ZnO filled FDM lattice template with inset showing the photodetector fabricated using FDM lattice template, and (d) Carbonized DLP printed lattice structure with inset showing the distribution of pore size.

Another functionality of the present study can be found in designing lattice structures which can find applications as templates hosting

nanomaterials, fillers for realizing sensors, resonators, and filters [8, 66-67]. Also, chemical and thermal modification of such lattice structures can be used for applications as electrodes for batteries, fuel cells, and catalytic converters [68].

Figure 7 shows the lattice structures printed by both FDM and DLP 3D printing techniques with optimized pore size for high resolution along with their functionality. Figure 7a shows the lattice structure printed by FDM using PLA thermoplastic with an inset showing a histogram analysis of pore distribution. The mean pore size calculated from the analysis is ~ 650 µm. Similarly, the lattice structure printed by DLP using PUAR resin with histogram analysis of the pore distribution is shown in Figure 7b, and from the analysis the pore size is ~ 220 µm. Dimension and layer number of different sizes of ring electrode and lattice structure for both the techniques are given in the Table 4.

Table 4: Details of stamps and lattice structure printed by DLP and FDM techniques.

Ring Electrode						
Parameters	FDM			DLP		
Configuration	S	M	L	S	M	L
Inner ring radius (µm)	1580	1630	3792	738	891	1270
Outer ring radius (µm)	2850	2985	2575	1204	1550	1985
Total number of layer	10	12	14	20	24	28
Layer height (µm)	100			50		
Lattice structure						
Pore Size	650 µm			220 µm		
Number of layer	20			40		

Figure 7c shows the lattice structure used as a template hosting ZnO nanoparticles. Such templates filled with nanomaterials have potential applications for fabricating out-of-plane optical sensors, strain sensors, and triboelectric generators. The inset shows the device configuration of the out-of-plane photodetector. Figure 7d shows the carbonization of the lattice structure as shown in Figure 7b. Being a thermosetting polymer, the carbonization at 1200 °C results in a conductive lattice structure having potential application as an electrode for batteries and fuel cells. The inset of Figure 7d shows the histogram analysis of the pore size after carbonization, indicating the pore size is ~ 160 µm and a shrinkage in lattice size by ~ 27 %. The distinguishing aspects of the comparative study are the quantification of void volume due to the staircase effect and comparing both techniques for specific applications like stamps for electrode printing. Also, the edge sharpness is another distinct aspect that plays a major role in designing mechanical parts for tool matching and compatibility with the hosting system. Further the comparative study can be optimized for selective adoption of the technique and models for specific application which pertains to minimizing staircase effect, optimizing tessellation, better slicing and also instrument parameters like LED affluence, pixel density and material properties like minimizing warping and photoinitiator for high resolution.

4. CONCLUSION

A simple artifact based on a pyramid is used for comparative analysis of FDM and DLP printing techniques. The dependence on process parameters during slicing is studied for surface finish and print resolution.

- **Dimensional Accuracy:** The FDM-printed pyramid exhibited an average layer thickness of ~104 µm, whereas the DLP-printed pyramid had a much finer layer thickness of ~54 µm.
- **Staircase Effect**: The void volume due to the staircase effect was calculated to be ~2.9% for FDM and only ~0.14% for DLP, indicating better surface finish and dimensional accuracy in DLP-printed samples.
- **Edge Sharpness and Print Resolution**: DLP-printed samples exhibited superior edge sharpness and print resolution compared to their FDM counterparts. This resulted in more precise and cleaner geometries, particularly noticeable in fine-feature details.
- **Mechanical Properties**: Mechanical testing showed that the MOE for FDM-printed samples was 1.7 GPa, with UTS of 62 MPa, exhibiting anisotropic behavior. In contrast, DLP-printed

samples demonstrated isotropic properties with an MOE of ~950 MPa and UTS of ~39 MPa.

- **Degree of Anisotropy (DOA)**: The FDM-printed samples showed a DOA of 0.35, indicating significant orientation-dependent mechanical properties. DLP samples, however, exhibited more consistent isotropic behavior across the structure.
- **Electrode Dimensions**: Systematic analysis of co-centric ring electrodes printed using FDM and DLP revealed that the active area of FDM imprints was 17 times larger compared to DLP-printed electrodes, indicating substantial differences in resolution and feature size across all stamp sizes.
- **Lattice Structure Analysis**: FDM-printed lattice structures showed a mean pore size of ~650 µm, while the DLP-printed lattice structures using PUAR resin had a significantly smaller pore size of ~220 µm. This highlights the variability in structural characteristics and print quality depending on the chosen printing technique.

ACKNOWLEDGES

Mr. Bhanu Prakash Bisht acknowledges Council of Scientific and Industrial Research (CSIR) & Academy of Scientific and Innovative Research (AcSIR) for fellowship and academic support. Dr. Vijaykumar Toutam acknowledges CSIR for financial support under Lab Project and in house R &D support.

REFERENCES

1. D. Godec et al., "Introduction to Additive Manufacturing," Pages 1–44, 2022.

2. "ISO/ASTM 52900:2021(en), Additive manufacturing — General principles — Fundamentals and vocabulary." Accessed: Nov. 27, 2023. [Online]. Available: https://www.iso.org/obp/ui/#iso:std:iso-astm:52900:ed-2:v1:en

3. Citarella R., Giannella V., "Additive Manufacturing in Industry," Applied Sciences, Vol. 11, Issue 2, Pages 840, 2021.

4. Dhinakaran V., Kumar K. P. M., Ram P. M. B., Ravichandran M., Vinayagamoorthy M., "A review on recent advancements in fused deposition modeling," Mater Today Proc, Vol. 27, Pages 752–756, 2020.

5. Kristiawan R. B., Imaduddin F., Ariawan D., Ubaidillah, Arifin Z., "A review on the fused deposition modeling (FDM) 3D printing: Filament processing, materials, and printing parameters," Open Engineering, Vol. 11, Issue 1, Pages 639–649, 2021.

6. Patel A., Taufik M., "A study on design and development of prosthetics by fused deposition modelling," The Fourth Scientific Conference for Electrical Engineering Techniques Research (EETR2022), Vol. 2804, Issue 1, Pages 020144, 2023.

7. Foster C. W., et al., "3D Printed Graphene Based Energy Storage Devices," Scientific Reports, Vol. 7, Issue 1, Pages 1–11, 2017.

8. Bisht B. P., Toutam V., Dhakate S. R., "3D Printed Lattice Template by Material Extrusion Technique for Fabrication of Pixelated Photodetector," 3D Printing and Additive Manufacturing, Vol. 10, Issue 6, Pages 74–83, 2023.

9. Mallikarjuna B., Bhargav P., Hiremath S., Jayachristiyan K. G., Jayanth N., "A review on the melt extrusion-based fused deposition modeling (FDM): background, materials, process parameters and military applications," International Journal on Interactive Design and Manufacturing (IJIDeM) 2023, Pages 1–15, 2023.

10. Parulski C., Jennotte O., Lechanteur A., Evrard B., "Challenges of fused deposition modeling 3D printing in pharmaceutical applications: Where are we now?," Adv Drug Deliv Rev, Vol. 175, Pages 113810, 2021.

11. Baechle-Clayton M., Loos E., Taheri M., Taheri H., "Failures and Flaws in Fused Deposition Modeling (FDM) Additively Manufactured Polymers and Composites," Journal of Composites Science, Vol. 6, Issue 7, Page 202, 2022.

12. Pagac M., et al., "A Review of Vat Photopolymerization Technology: Materials, Applications, Challenges, and Future Trends of 3D Printing," Polymers, Vol. 13, Issue 4, Page 598, 2021.

13. Mu Q., et al., "Digital light processing 3D printing of conductive complex structures," Addit Manuf, Vol. 18, Pages 74–83, 2017.

14. Chaudhary R., Fabbri P., Leoni E., Mazzanti F., Akbari R., Antonini C., "Additive manufacturing by digital light processing: a review," Progress in Additive Manufacturing, Vol. 8, Issue 2, Pages 331–351, 2022.

15. Bagheri A., Jin J., "Photopolymerization in 3D Printing," ACS Appl Polym Mater, Vol. 1, Issue 4, Pages 593–611, 2019.

16. Shah M., et al., "Vat photopolymerization-based 3D printing of polymer nanocomposites: current trends and applications," RSC Adv, Vol. 13, Issue 2, Pages 1456–1496, 2023.

17. Colella R., Chietera F. P., Catarinucci L., "Analysis of FDM and DLP 3D-Printing Technologies to Prototype Electromagnetic Devices for RFID Applications," Sensors, Vol. 21, Issue 3, Page 897, 2021.

18. Bisht B. P., et al., "3D printed ZnO-Polyurethane acrylate resin composite for wide spectral photo response optical detectors," Sens Actuators A Phys, Vol. 351, Page 114165, 2023.

19. Quan H., Zhang T., Xu H., Luo S., Nie J., Zhu X., "Photo-curing 3D printing technique and its challenges," Bioact Mater, Vol. 5, Issue 1, Pages 110–115, 2020.

20. Stefaniak A. B., et al., "Particle and vapor emissions from vat polymerization desktop-scale 3-dimensional printers," J Occup Environ Hyg, Vol. 16, Issue 8, Page 519, 2019.

21. Kuznetsov V. E., Tavitov A. G., Urzhumtsev O. D., Mikhalin M. V., Moiseev A. I., "Hardware Factors Influencing Strength of Parts Obtained by Fused Filament Fabrication," Polymers, Vol. 11, Issue 11, Page 1870, 2019.

22. Gao X., Qi S., Kuang X., Su Y., Li J., Wang D., "Fused filament fabrication of polymer materials: A review of interlayer bond," Addit Manuf, Vol. 37, Page 101658, 2021.

23. Ferretti P., et al., "Relationship between FDM 3D Printing Parameters Study: Parameter Optimization for Lower Defects," Polymers, Vol. 13, Issue 13, Page 2190, 2021.

24. Bakhtiari H., Nikzad M., Tolouei-Rad M., "Influence of Three-Dimensional Printing Parameters on Compressive Properties and Surface Smoothness of Polylactic Acid Specimens," Polymers, Vol. 15, Issue 18, Page 3827, 2023.

25. Bouzaglou O., Golan O., Lachman N., "Process Design and Parameters Interaction in Material Extrusion 3D Printing: A Review," Polymers (Basel), Vol. 15, Issue 10, 2023.

26. Harun N. H., Kasim M. S., Abidin M. Z. Z., Izamshah R., Attan H., Ganesan H. N., "A Study on Surface Roughness During Fused Deposition Modelling: A Review," Journal of Advanced Manufacturing Technology (JAMT), Vol. 12, Issue 1, Pages 25–36, 2018.

27. Brighenti R., Marsavina L., Marghitas M. P., Montanari M., Spagnoli A., Tatar F., "The effect of process parameters on mechanical characteristics of specimens obtained via DLP additive manufacturing technology," Mater Today Proc, Vol. 78, Pages 331–336, 2023.

28. Zhang Z., Li P. L., Chu F. T., Shen G., "Influence of the three-dimensional printing technique and printing layer thickness on model accuracy," Journal of Orofacial Orthopedics, Vol. 80, Issue 4, Pages 194–204, 2019.

29. Jiang T., et al., "Study of Forming Performance and Characterization of DLP 3D Printed Parts," Materials, Vol. 16, Issue 10, Page 3847, 2023.

30. Mohamed O. A., Masood S. H., Bhowmik J. L., Blaj M., Oancea G., "Fused deposition modelling process: a literature review," IOP Conf Ser Mater Sci Eng, Vol. 1009, Issue 1, Page 012006, 2021.

31. Ligon S. C., Liska R., Stampfl J., Gurr M., Mülhaupt R., "Polymers for 3D Printing and Customized Additive Manufacturing," Chem Rev, Vol. 117, Issue 15, Pages 10212–10290, 2017.

32. C. Kittel and P. McEuen, "Introduction to solid state physics", Pages 692.

33. "Ecological pyramid - Wikiwand." Accessed: Nov. 28, 2023. [Online]. Available: https://www.wikiwand.com/en/Ecological_pyramid

34. Wikiwand, "Square pyramid," [Online]. Available: https://www.wikiwand.com/en/Square_pyramid, November 28, 2023.

35. Bochmann L., Bayley C., Helu M., Transchel R., Wegener K., Dornfeld D., "Understanding error generation in fused deposition modeling," Surf Topogr, Vol. 3, Issue 1, Page 014002, 2015.

36. Alexopoulou V. E., Christodoulou I. T., Markopoulos A. P., "Effect of Printing Speed and Layer Height on Geometrical Accuracy of FDM-Printed Resolution Holes of PETG Artifacts," Engineering Proceedings, Vol. 24, Issue 1, Page 11, 2022.

37. Mac G., Pearce H., Karri R., Gupta N., "Uncertainty quantification in dimensions dataset of additive manufactured NIST standard test artifact," Data Brief, Vol. 38, Page 107286, 2021.

38. Huang J., Zhang B., Xiao J., Zhang Q., "An Approach to Improve the Resolution of DLP 3D Printing by Parallel Mechanism," Applied Sciences, Vol. 12, Issue 24, Page 12905, 2022.

39. Manizani S. M., Zamani J., Salehi M., Shayesteh M. T., "Investigating the Effect of Separation Speed and Image Cross-Section Geometry on The Separation Force in DLP Method using FEP and PP Polymer Membranes," International Journal of Advanced Design and Manufacturing Technology, Vol. 64, Issue 3, Page 9, 2023.

40. Grzebieluch W., Grajzer M., Mikulewicz M., "Comparative Analysis of Fused Deposition Modeling and Digital Light Processing Techniques for Dimensional Accuracy in Clear Aligner Manufacturing," Med Sci Monit, Vol. 29, Page e940922, 2023.

41. Lendvai L., Fekete I., Rigotti D., Pegoretti A., "Experimental study on the effect of filament-extrusion rate on the structural, mechanical and thermal properties of material extrusion 3D-printed polylactic acid (PLA) products," Progress in Additive Manufacturing, Pages 1–11, 2024.

42. Yang Y., Zhou Y., Lin X., Yang Q., Yang G., "Printability of External and Internal Structures Based on Digital Light Processing 3D Printing Technique," Pharmaceutics, Vol. 12, Issue 3, Pages 207, 2020.

43. Council of Scientific & Industrial Research, "CSIR Logo | Council of Scientific & Industrial Research," https://www.csir.res.in/csir-logo, November 28, 2023.

44. "National Physical Laboratory of India - Wikiwand," https://www.wikiwand.com/en/National_Physical_Laboratory_of_India, November 28, 2023.

45. "Online SVG image converter," https://image.online-convert.com/convert-to-svg, November 28, 2023.

46. "Thingiverse - Digital Designs for Physical Objects," https://www.thingiverse.com/, November 28, 2023.

47. "SVG 2 STL," https://svg2stl.com/, November 28, 2023.

48. Alsoufi M. S., Elsayed A. E., "How Surface Roughness Performance of Printed Parts Manufactured by Desktop FDM 3D Printer with PLA+ is Influenced by Measuring Direction," Vol. 5, Issue 5, 2017.

49. Duan K., et al., "Monolithically 3D-Printed Microfluidics with Embedded µTesla Pump," Micromachines (Basel), Vol. 14, Issue 2, Page 237, 2023.

50. Luo Z., et al., "Digital light processing 3D printing for microfluidic chips with enhanced resolution via dosing- and zoning-controlled vat photopolymerization," Microsystems & Nanoengineering, Vol. 9, Issue 1, Pages 1–13, 2023.

51. Wu Y., Su H., Li M., Xing H., "Digital light processing-based multi-material bioprinting: Processes, applications, and perspectives," J Biomed Mater Res A, Vol. 111, Issue 4, Pages 527–542, 2023.

52. International Organization for Standardization, "ISO/ASTM 52921:2013 - Standard terminology for additive manufacturing — Coordinate systems and test methodologies," https://www.iso.org/standard/62794.html, November 28, 2023.

53. Corapi D., Morettini G., Pascoletti G., Zitelli C., "Characterization of a Polylactic acid (PLA) produced by Fused Deposition Modeling (FDM) technology," Procedia Structural Integrity, Vol. 24, Pages 289–295, 2019.

54. Farkas A. Z., Galatanu S. V., Nagib R., "The Influence of Printing Layer Thickness and Orientation on the Mechanical Properties of DLP 3D-Printed Dental Resin," Polymers 2023, Vol. 15, Issue 5, Page 1113, 2023.

55. Cojocaru V., Frunzaverde D., Miclosina C. O., Marginean G., "The Influence of the Process Parameters on the Mechanical Properties of PLA Specimens Produced by Fused Filament Fabrication—A Review," Polymers, Vol. 14, Issue 5, Page 886, 2022.

56. Susanto B., et al., "Investigating Microstructural and Mechanical Behavior of DLP-Printed Nickel Microparticle Composites," Journal of Composites Science, Vol. 8, Issue 7, Page 247, 2024.

57. Dhand A. P., Davidson M. D., Zlotnick H. M., Kolibaba T. J., Killgore J. P., Burdick J. A., "Additive manufacturing of highly entangled polymer networks," Science, Vol. 385, Issue 6708, Pages 566–572, 2024.

58. Bisht B. P., et al., "3D printed ZnO-Polyurethane acrylate resin composite for wide spectral photo response optical detectors," Sens Actuators A Phys, Vol. 351, Page 114165, 2023.

59. Khosravani M. R., Soltani P., Reinicke T., "Effects of steps on the load bearing capacity of 3D-printed single lap joints," Journal of Materials

Research and Technology, Vol. 23, Pages 1834–1847, 2023.

60. Zhang J., Hu Q., Wang S., Tao J., Gou M., "Digital Light Processing Based Three-dimensional Printing for Medical Applications," Int J Bioprint, Vol. 6, Issue 1, Pages 12–27, 2020.

61. Gonzalez-Fernandez T., Tenorio A. J., Leach J. Kent, "Three-Dimensional Printed Stamps for the Fabrication of Patterned Microwells and High-Throughput Production of Homogeneous Cell Spheroids," 3D Print Addit Manuf, Vol. 7, Issue 3, Pages 139–147, 2020.

62. Pinheiro A. C. Nava, Ferreira V. Souza, Lucca B. Gabriel, "Stamping method based on 3D printing and disposable napkin: Cheap production of paper analytical devices for alcohol determination in beverages aiming forensics and food control," Microchemical Journal, Vol. 180, Page 107604, 2022.

63. Stromberg L. R., et al., "Stamped multilayer graphene laminates for disposable in-field electrodes: application to electrochemical sensing of hydrogen peroxide and glucose," Microchimica Acta, Vol. 186, Issue 8, Pages 1–13, 2019.

64. Araujo T. A. de, Moraes N. C. de, Petroni J. M., Ferreira V. S., Lucca B. G., "Simple, fast, and instrumentless fabrication of paper analytical devices by novel contact stamping method based on acrylic varnish and 3D printing," Microchimica Acta, Vol. 188, Issue 12, Pages 1–11, 2021.

65. Ali M., Alam F., Ahmed I., AlQattan B., Yetisen A. K., Butt H., "3D printing of Fresnel lenses with wavelength selective tinted materials," Addit Manuf, Vol. 47, Page 102281, 2021.

66. Chen H., Guo L., Zhu W., Li C., "Recent Advances in Multi-Material 3D Printing of Functional Ceramic Devices," Polymers, Vol. 14, Issue 21, Page 4635, 2022.

67. Yan L., Zhu K., Zhang Y., Zhang C., Zheng X., "Effect of Absorbent Foam Filling on Mechanical Behaviors of 3D-Printed Honeycombs," Polymers, Vol. 12, Issue 9, Page 2059, 2020.

68. Khan S. A., Rahman M. A., Khraisheh M., Hassan I. G., "Advances in 3D printed periodic lattice structures for energy research: Energy storage, transport and conversion applications," Mater Des, Vol. 239, Page 112773, 2024.